scientific reports

OPEN

Prediction of topological Dirac semimetal in Ca-based Zintl layered compounds CaM$_2$X$_2$ (M = Zn or Cd; X = N, P, As, Sb, or Bi)

Liang-Ying Feng[1], Rovi Angelo B. Villaos[1], Aniceto B. Maghirang III[1], Zhi-Quan Huang[1], Chia-Hsiu Hsu[1,2], Hsin Lin[3] & Feng-Chuan Chuang[1,2,4,5✉]

Topological Dirac materials are attracting a lot of attention because they offer exotic physical phenomena. An exhaustive search coupled with first-principles calculations was implemented to investigate 10 Zintl compounds with a chemical formula of CaM$_2$X$_2$ (M = Zn or Cd, X = N, P, As, Sb, or Bi) under three crystal structures: CaAl$_2$Si$_2$-, ThCr$_2$Si$_2$-, and BaCu$_2$S$_2$-type crystal phases. All of the materials were found to energetically prefer the CaAl$_2$Si$_2$-type structure based on total ground state energy calculations. Symmetry-based indicators are used to evaluate their topological properties. Interestingly, we found that CaM$_2$Bi$_2$ (M = Zn or Cd) are topological crystalline insulators. Further calculations under the hybrid functional approach and analysis using $k \cdot p$ model reveal that they exhibit topological Dirac semimetal (TDSM) states, where the four-fold degenerate Dirac points are located along the high symmetry line in-between Γ to A points. These findings are verified through Green's function surface state calculations under HSE06. Finally, phonon spectra calculations revealed that CaCd$_2$Bi$_2$ is thermodynamically stable. The Zintl phase of AM$_2$X$_2$ compounds have not been identified in any topological material databases, thus can be a new playground in the search for new topological materials.

The investigations on topological materials (TMs) have been steadily gaining traction in the field of materials physics because they exhibit novel physical phenomena[1,2]. Intriguingly, the topological Dirac semimetal (TDSM) is an intermediate quantum state between trivial and non-trivial states[3]. Also, these new types of materials are a good playground to identify the new quantum phenomena in condensed matter physics from Dirac semimetals to Weyl semimetals[4,5]. TDSM is observed when the valence and conduction bands are degenerate at one critical point, defined as Dirac point in 3-dimension (3D) bulk structure near the Fermi level, and exhibits Lorentz symmetry breaking, which forms a Dirac cone[6,7]. Different types of cones at the Dirac point with or without inverse-sign slopes can be classified into either type I or type II Dirac semimetal, respectively[8]. TDSM has attracted significant attention because of its physical properties such as giant diamagnetism[9,10], quantum magnetoresistance[11–14], characteristic Landau level structures, and oscillating quantum spin Hall effect[15,16]. Recently, the TDSM state of materials has been experimentally observed in Cd$_3$As$_2$[14,17–20] and Na$_3$Bi[13,21] as a type I Dirac semimetal. On the other hand, some of the transition metal dichalcogenides (TMDs) were proposed as a type II Dirac semimetal, such as PtSe$_2$[22,23], PdTe$_2$[24,25], PtTe$_2$[26,27], and NiTe$_2$[28–31], and were verified through angle-resolved photoemission spectroscopy (ARPES) experiments. In addition, numerous studies have demonstrated that compounds with hexagonal structure exhibit interesting electronic [32,33,34], and topological properties[35–39,40–42].

Meanwhile, a group of materials called the Zintl compounds, named after Eduard Zintl who discovered them[43], are receiving recognition in materials physics because of their applications in thermoelectric (TE) devices[44]. As more compounds were discovered, a more general description of these materials are now based on electron transfer between the alkali or alkaline earth cation and the electronegative elements which results in a filled valence shells through covalent bonding or formation of lone electron pairs. Therefore, these phases possess salt-like characteristics from the ionic bonding between the cation and the anion[43]. This definition of

[1]Department of Physics, National Sun Yat-Sen University, 70 Lienhai Rd., Kaohsiung 80424, Taiwan. [2]Physics Division, National Center for Theoretical Sciences, Taipei 10617, Taiwan. [3]Institute of Physics, Academia Sinica, Taipei 115201, Taiwan. [4]Department of Physics, National Tsing Hua University, Hsinchu 30013, Taiwan. [5]Center for Theoretical and Computational Physics, National Sun Yat-Sen University, Kaohsiung 80424, Taiwan. ✉email: fchuang@mail.nsysu.edu.tw
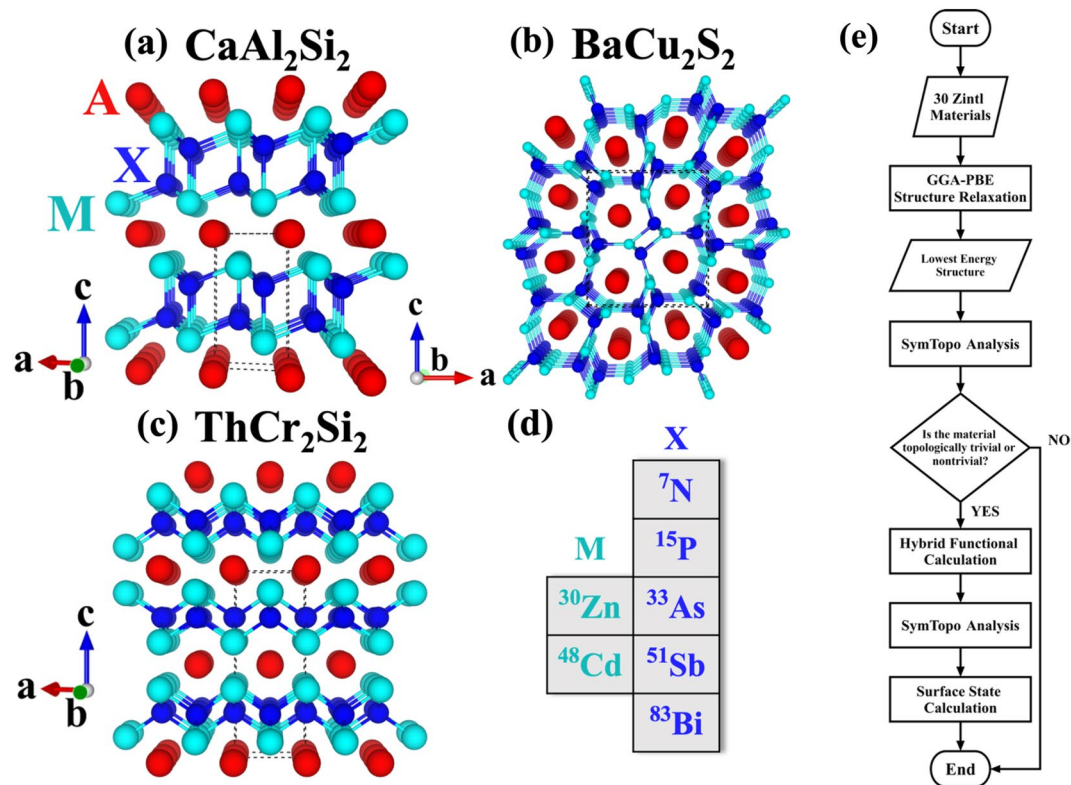
Figure 1. Three possible structures of bulk AM_2X_2: (**a**) $CaAl_2Si_2$-type ($P\bar{3}m1$, 164) (**b**) $BaCu_2S_2$-type (Pnma, 62) (**c**) $ThCr_2Si_2$-type (I4/mmm, 139). (**d**) The list of elements used in this exhaustive materials search. M and X are, Group IIB, and Group VA, respectively. (**e**) The flow chart of our search for identifying the topological materials.

Zintl phase is a description of ionic and covalent bonding within intermetallic phases which provides insight on their structure and properties[45]. Recently, Zintl phases have been used as thermoelectric materials because of their structural complexity, low lattice thermal conductivity, and excellent stability at high temperature. Interestingly, some of the TE materials may exhibit topological properties due to their strong spin–orbit coupling (SOC) effect and small bandgap[46]. Interestingly, a new group of Zintl materials[47–51] have been attracting attention because of their possible applications in the design and discovery of new quantum materials. Specifically, $EuSn_2P_2$[47] and $EuCd_2As_2$[48] have been recently experimentally and theoretically investigated. It was found that $EuSn_2P_2$ is antiferromagnetic and is an energetically stable state at low temperatures. Moreover, it was found to be an antiferromagnetic (AFM) topological insulator with Dirac-like surface states near the Fermi level. Similar to $EuSn_2P_2$, $EuCd_2As_2$ is also an antiferromagnet that exhibits three different types of non-trivial properties: axion insulator, AFM topological crystalline insulator (TCI), and higher order topological insulator. With these findings, $EuCd_2As_2$ is the first experimentally realized magnetic TDSM. In addition to these two materials, $EuIn_2As_2$[49] and $EuCd_2Bi_2$[50] have been theoretically predicted to exhibit magnetic topological insulator phase. These materials belong to a new group of exotic quantum materials known as axionic insulators[52,53]. With these exciting new findings in the Zintl compounds, it is crucial that an in-depth material search should be conducted to further explore this new playground of materials.

In this study, we investigate the 10 Zintl phase materials which have a general chemical formula of CaM_2X_2, where M = Cd or Zn, and X = N, P, As, Sb, or Bi. Through ground state energy and phonon dispersion calculations, we determined the most energetically favorable structure and found that all of these materials only adapt the hexagonal $CaAl_2Si_2$-type layered structure. Thus, we only focused on this layered-structure phase. Symmetry-based indicators are then used to evaluate their topological properties. Surprisingly, we found that CaM_2Bi_2 (M = Zn or Cd) are topological crystalline insulators (TCIs) under the GGA-PBE. Further calculations under the hybrid functional approach and analysis using $k \cdot p$ model reveal that they exhibit topological Dirac semimetal (TDSM) states, where the four-fold degenerate Dirac points are located along the high symmetry line in-between Γ to A points. Our findings show that the Zintl phase of AM_2X_2 compounds can be a new playground in the search for new topological materials (TMs).

Results and discussion

The AM_2X_2 Zintl compounds could exhibit three known structures: trigonal $CaAl_2Si_2$-type structure ($P\bar{3}m1$, 164), orthorhombic $BaCu_2S_2$-type structure (Pnma, 62), and tetragonal $ThCr_2Si_2$-type structure (I4/mmm, 139), as shown in Fig. 1a–c, respectively[44]. The elements of CaM_2X_2 used in our study are shown in Fig. 1d. The M are Zn or Cd from Group 2B (Zinc Group), and X are N, P, As, Sb, or Bi from Group 5A (Pnictogen Group).
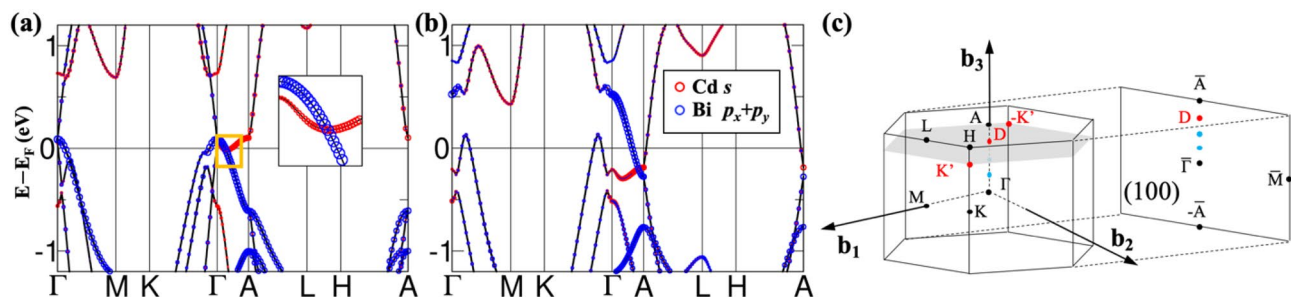
Figure 2. The band structures of bulk CaCd$_2$Bi$_2$ under HSE06 (**a**) w/o SOC and (**b**) with SOC. The circle corresponds to the orbital contribution from Cd s orbital and Bi p_x and p_y orbitals indicated by red and blue, respectively. To identify the bands near Γ point of (**a**), the zoom-in diagram was provided in the inset. (**c**) The corresponding 3D first Brillouin zone (BZ) of the CaAl$_2$Si$_2$-type structure and the projected surface BZ at (100) plane. The high-symmetry points and Dirac points (red for CaCd$_2$Bi$_2$ and blue for CaCd$_2$SbBi) are labeled in the figure.

The CaAl$_2$Si$_2$-type structure is stacked along the c-direction by two-layer structures A^{2+} and [M$_2$X$_2$]$^{2-}$. On the other hand, the orthorhombic BaCu$_2$S$_2$-type structure is formed through the covalent bonding between M and X. This results in a channel-like structure along the lattice vector b with A atoms inside these channels as shown in Fig. 1b. Finally, the ThCr$_2$Si$_2$-type structure is composed of negatively charged layers of MX$_4$ tetrahedra and positively charged A layers, stacked along the c direction. The MX$_4$ tetrahedra layers contain strong covalent M–X bonds and weaker M–M interactions, while an ionic bonding exists between A and the MX$_4$ tetrahedra layers[54].

To systematically study the 10 Zintl compounds, the exhaustive search approach is adapted. The procedures are depicted in the flowchart shown in Fig. 1e. First, we assigned the 10 compounds to the three known structures in the literature, totaling to 30 materials, and determined the most stable structure of each compound using the GGA-PBE functional. Second, the topological properties of the 10 compounds with the lowest ground state energy structure were determined using the SymTopo program[55] via the symmetry-indicator analysis. The band structures were also calculated to determine their electronic properties: insulating, semi-metallic, or metallic. Third, hybrid functional calculations combined with the SymTopo program[55] were used again to verify their topological and electronic properties. Finally, the evidence of topological properties is further explored through the surface Green's function calculations.

The results of the exhaustive search procedure, as well as the topological phases of each material are summarized in Supplementary Table S1 (without SOC) and S2 (with SOC). For the 10 compounds considered, they all adapt the CaAl$_2$Si$_2$-type structure. Nevertheless, the bulk band structures for the BaCu$_2$S$_2$-type and ThCr$_2$Si$_2$-type CaM$_2$X$_2$ compounds considered in this study are shown in Supplementary Figures S1 to S4. The SymTopo analysis indicated that two compounds, CaZn$_2$Bi$_2$ and CaCd$_2$Bi$_2$, are found to be TCSMs, and CaCd$_2$N$_2$ would be TSM while the rest are trivial topological properties under GGA. Moreover, phonon dispersion calculations were performed to verify the thermodynamic stability of the CaAl$_2$Si$_2$-type CaM$_2$X$_2$ compounds (See Figure S5). As seen in Figure S5, majority of the bulk materials, except for CaZn$_2$Bi$_2$, considered in this study have no imaginary phonon frequencies indicating thermodynamic stability. On the other hand, CaZn$_2$Bi$_2$ in CaAl$_2$Si$_2$-type exhibits imaginary phonon frequencies and is thermodynamically unstable, implying it may adopt another stable structure. Interestingly, the monolayer CaZn$_2$Bi$_2$ is stable, as demonstrated in another study[56]. Focusing on CaCd$_2$Bi$_2$, Figure S5 shows that CaCd$_2$Bi$_2$ is thermodynamically stable, implying possible experimental synthesis. Also, the phase diagrams for CaCd$_2$Sb$_2$ and CaCd$_2$Bi$_2$ from the Open Quantum Materials Database[57,58] show that both materials have negative formation energies, implying relative stability. Furthermore, experimental realization of this material is indeed possible since CaCd$_2$Sb$_2$ with similar crystal structure have already been synthesized[59]. Intriguingly, these materials have not been identified in several topological material databases[60–62]. The band structures of these 10 compounds are shown in Supplementary Figure S6 and S7. To verify the results, all the compounds are recalculated again with HSE06 as shown in Figures S8 and S9. Interestingly, CaCd$_2$Bi$_2$ and CaZn$_2$Bi$_2$ are found to be TDSM, while the other 8 materials just have trivial insulating phase. To demonstrate the topological properties of these two materials, we choose CaCd$_2$Bi$_2$ as the representative material for the rest of our discussion.

As seen in Supplementary Table S1 and Figures S6 (a, c, e, g, and i) and S7 (a, c, e, g, and i) under GGA-PBE without SOC, the SymTopo results and band structures, respectively, reveal that CaCd$_2$Sb$_2$ is a trivial insulator (Figure S7g) while CaCd$_2$Bi$_2$ is a topological semimetal (TSM) (Figure S7i). When turning on SOC, CaCd$_2$Sb$_2$ is a trivial semimetal (SM) (Figure S7h), while CaCd$_2$Bi$_2$ is a topological crystalline semimetal (TCSM) (Figure S7j). Here, the observed transition from trivial SM to TCSM in CaCd$_2$Bi$_2$ is due to the SOC effect, meaning the bands are gapped between Γ to A. In order to understand the evolution of topological phase transitions, the SOC strength of CaCd$_2$Bi$_2$ is varied from 0 to 1. The bands gradually open at two symmetry points, one is at Γ while the other is at A point, as the SOC strength increases. This band opening explains the mechanism behind the TCSM property of CaCd$_2$Bi$_2$ (see Supplementary Figures S10 and S11). This similar behavior is also observed in Sb/Bi planar honeycomb which exhibits topological crystalline insulator phase[63].

Moving on to the results under the hybrid functional approach, we show in Fig. 2a, b the band structures of CaCd$_2$Bi$_2$ under HSE06 with and without SOC. Since HSE06 has been proven to be more superior than the standard GGA-PBE functional, we will focus only on HSE06 results for the succeeding discussions unless mentioned
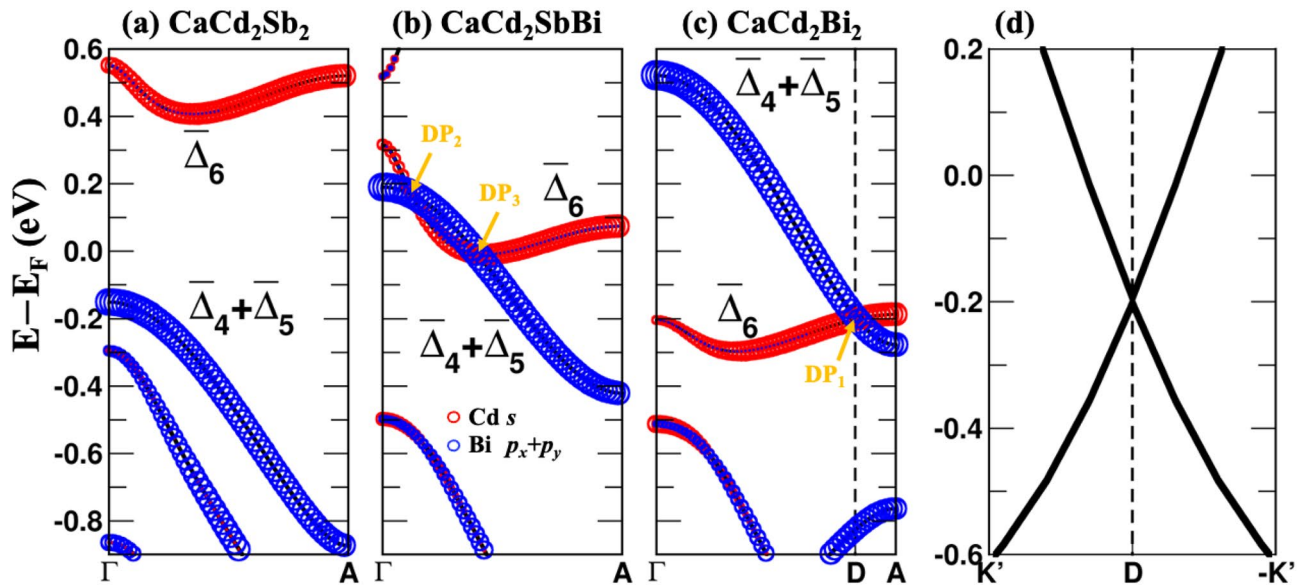
Figure 3. (**a–c**) The HSE06 with SOC band structures of $CaCd_2Sb_2$, $CaCd_2SbBi$, and $CaCd_2Bi_2$. The circle corresponds to the orbital contribution from Cd s orbital and Bi p_x and p_y orbitals indicated by red and blue, respectively. The irreducible representations are labeled as $\overline{\Delta}_6$ and $\overline{\Delta}_4 + \overline{\Delta}_5$. The three Dirac points are labeled in orange arrows (DP_1, DP_2, and DP_3). (**d**) Zoomed-in view of the band path near passing the Dirac cone of $CaCd_2Bi_2$ along the -K' to D to K'.

otherwise. Interestingly, $CaCd_2Bi_2$ is a TSM without SOC (Fig. 2a) exhibited the characteristics of a nodal line semimetal with degenerate state (bands are contributed by Bi p_x and p_y orbitals) along Γ to A as highlighted by the yellow square, but became a TDSM under SOC (Fig. 2b) with a Dirac point crossing observed along Γ to A. The locations of Dirac points are in red labeled in Fig. 2c.

To understand the mechanism behind the existence of the Dirac point, the zoomed-in with SOC band structures of $CaCd_2Sb_2$ and $CaCd_2Bi_2$ along Γ to A are shown in Fig. 3a, c. For $CaCd_2Sb_2$, there exists a band opening with a gap of 0.55 eV resulting in a trivial insulator phase. In contrast, $CaCd_2Bi_2$ demonstrates gapless linear bands crossing in (0, 0, $k_D \approx \pm 0.4152\pi/c$) at the energy level of $E - E_F \approx -0.20$ eV. It is a four-fold degenerate Dirac point (DP_1) belonging to two different irreducible representations ($\overline{\Delta}_4 + \overline{\Delta}_5$ and $\overline{\Delta}_6$) which prohibits hybridization, as shown in Fig. 3c. To prove that it is indeed a 3D Dirac point, we show in Fig. 3d the band path passing the Dirac cone of $CaCd_2Bi_2$ along the DP_1 to -K' and DP_1 to K', which is perpendicular to Γ to A direction. This result demonstrated the existence of a TDSM state in $CaCd_2Bi_2$. The Dirac point (DP_1) is protected by the C_3 rotational symmetry about the c axis.

To explore the topological phase transition due to SOC strength and doping, we propose a hypothetical material $CaCd_2SbBi$ that has an equal concentration of Sb and Bi. In $CaCd_2SbBi$, Bi doping breaks the inversion symmetry of the system. The $CaCd_2SbBi$ in $CaAl_2Si_2$-type structure belongs to the space group $P\overline{3}m1$ (164), while the doped case belongs to P3m1 (156). For comparison, Fig. 3b also shows the band structure of $CaCd_2SbBi$ along the Γ to A under HSE06. Interestingly, the substituted Bi in $CaCd_2SbBi$ causes the breaking of the inversion symmetry while preserving the C_3 rotational symmetry along the z-axis. From Fig. 3a–c, we observed the down shift of $\overline{\Delta}_6$ and upward shift of $\overline{\Delta}_4 + \overline{\Delta}_5$. Two bands, $\overline{\Delta}_4 + \overline{\Delta}_5$ and $\overline{\Delta}_6$, near the Fermi level closed and crossed over the Fermi level resulting in a pair of Dirac points (DP_2 and DP_3) in the first BZ, as shown by a pair of the blue points labeled in Fig. 2c. Surprisingly, the symmetry indicators at Γ and A are still the same as $CaCd_2Sb_2$, thus resulting in a trivial insulator phase. Totally, four emerging Dirac points are formed along -A to Γ to A. Eventually, one Dirac point remains as the material is changed to $CaCd_2Bi_2$.

To further elucidate the mechanism behind the TDSM in $CaCd_2Bi_2$, the band crossing between Γ and A points is expressed as an effective Hamiltonian. To prove that the fourfold point is a Dirac point, an analysis using the $k \cdot p$ model is discussed. The four-band effective Hamiltonian obeys the following three symmetries: threefold rotation symmetry (C_3^+), mirror symmetry (σ_{1v}), and inversion and time reversal symmetry (IT)[64]. The irreducible representations of the four-band at D (Fig. 3c, d), $\overline{\Delta}_4 + \overline{\Delta}_5$ and $\overline{\Delta}_6$, are chosen as the basis set. Using the Pauli matrices σ_1, σ_2, σ_3, and 2×2 identity matrix σ_0, the matrix representations of the three symmetries for the basis are $-\sigma_0$, $i\sigma_3$, $-i\sigma_2$ and $\frac{1}{2}(\sigma_0 - i\sqrt{3}\sigma_2)$, $i\sigma_3$, $-i\sigma_2$, respectively. Thus, the four-band effective Hamiltonian takes the form

$$\begin{bmatrix} c_1 + c_2k_z + c_3k_z & 0 & c_4k_y - ic_5k_y & c_4k_x - ic_5k_x \\ 0 & c_1 + c_2k_z + c_3k_z & c_4k_x + ic_5k_x & -c_4k_y - ic_5k_y \\ c_4k_y + ic_5k_y & c_4k_x - ic_5k_x & c_1 + c_2k_z - c_3k_z & 0 \\ c_4k_x + ic_5k_x & -c_4k_y + ic_5k_y & 0 & c_1 + c_2k_z - c_3k_z \end{bmatrix}$$

The eigenvalues of the four-bands $(c_1 + c_2k_z) \pm \sqrt{(c_4^2 + c_5^2)k_x^2 + (c_4^2 + c_5^2)k_y^2 + c_3^2k_z^2}$ indicates that the four-fold point is indeed a Dirac point[64].

4
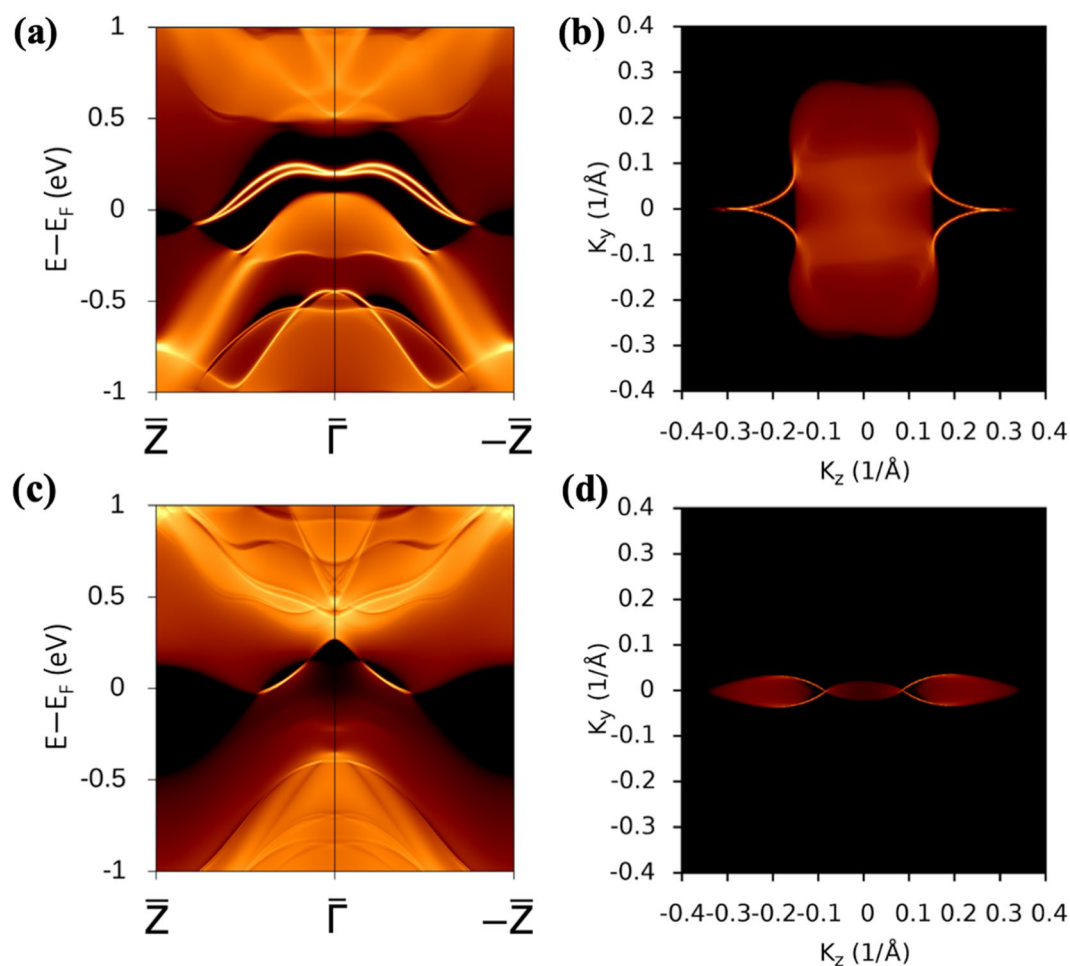
Figure 4. Bulk (**a**) $CaCd_2Bi_2$ and (**c**) $CaCd_2SbBi$ surface states projected on (100) plane under HSE06 with SOC. 2D Fermi arcs for (**b**) $CaCd_2Bi_2$ and (**d**) $CaCd_2SbBi$ at the $E-E_F = -0.1$ eV and 0.1 eV, respectively.

Finally, the Green's function-derived surface states projected on the (100) plane are calculated for $CaCd_2Bi_2$ (Fig. 4a) and $CaCd_2SbBi$ (Fig. 4c) to confirm the location of Dirac points. The 3D band structure is shown in Figure S12 highlighting two Dirac cones. The corresponding Fermi arcs highlighting the surface states of $CaCd_2Bi_2$ and $CaCd_2SbBi$ are shown in Fig. 4b, d, respectively. The connections to the Dirac points are projected onto different k locations in the surface BZ. The k points in the BZ projected on (100) surface are shown in Fig. 2c. The (100) surface of the Γ-centered BZ corresponds to the projection of the M-Γ line. In Fig. 4a, the calculated surface states connect two Dirac points (DP_1) in $CaCd_2Bi_2$ and cross at Γ point. However, since the structure of $CaCd_2SbBi$ breaks the inversion symmetry, four emerging Dirac points are formed. In Fig. 4c, the surface states of $CaCd_2SbBi$, in contrast with $CaCd_2Bi_2$, do not cross at a high symmetry point while connecting each pair of Dirac points (DP_2 and DP_3) in the BZ. The surface states connect the two Dirac points (DP_2 and DP_3) within Γ to A, while the other pair of surface states connect the two Dirac points within Γ to −A.

Methods

We systematically explored 10 compounds of CaM_2X_2 where M = Zn or Cd; and X = N, P, As, Sb, or Bi, under the three different existing structures, totaling 30 compounds of Zintl materials: $CaAl_2Si_2$-, $ThCr_2Si_2$-, and $BaCu_2S_2$-type crystal phase[44], through first-principles calculation as implemented in Vienna Ab initio Simulation Package (VASP) using projector-augmented wave (PAW) functions[65,66] under the Perdew-Burke-Ernzerhof (PBE)[67] functional with plane wave cut-off energy of 400 eV. The structures were allowed to relax until the residual Hellmann–Feynman forces acting on each atom were no greater than 10^{-2} eV/Å. The K-points sampling used is the Γ-centered grid Monkhorst–Pack with $24 \times 24 \times 12$ kmesh within the first Brillouin zone (BZ) for all the self-consistent calculations. Phonon spectra calculations are performed using the Phonopy[68] package. Spin-polarized and SOC were included in all the energetic calculations. In determining the magnetic properties, we treat magnetic moments (μ) greater than 0.1 as ferromagnetic (FM) states, while the rest are non-magnetic (NM) states. In NM state, we analyzed each case for the topological properties in 3D bulk structure using the SymTopo package[55] which uses symmetry-based indicators that can categorize different topological properties, such as trivial insulator (I), conventional metal (M), topological insulator (TI), topological crystalline insulator (TCI), high-symmetry-point semi-metal (HSPSM), and high-symmetry-line semi-metal (HSLSM). To predict

the topological properties of the investigate materials more accurately, Heyd-Scuseria-Ernzerhof (HSE06) hybrid functional[69] is further included in the band structure calculations. Finally, the Maximally-Localised Wannier Functions (MLWF) of CaM_2Bi_2 are obtained from the Wannier90[70] program, and the surface Green's function is calculated using the WannierTools program[71].

Conclusions

In this study, a systematic materials search coupled with first-principles calculations was performed to investigate 10 Zintl-phase compounds with a chemical formula of CaM_2X_2 (M = Zn or Cd; X = N, P, As, Sb, or Bi) and found all of these materials adapt $CaAl_2Si_2$-type structure. Symmetry-based indicators are used to evaluate their topological properties. Surprisingly, we found that CaM_2Bi_2 (M = Zn or Cd) are topological crystalline insulators (TCIs) under the GGA-PBE. Further calculations under the hybrid functional approach reveal that they exhibit topological Dirac semimetal (TDSM) states, where the four-fold degenerate Dirac points are located along the high symmetry line in-between Γ to A points and is analyzed using the effective Hamiltonian derived by the $k \cdot p$ model. These findings are verified through Green's function surface state calculations under HSE06. Finally, phonon calculations were done to verify the thermodynamic stability of the $CaCd_2Bi_2$, implying possible synthesis. Our findings show that the Zintl phase of AM_2X_2 compounds can be a new playground in the search for new topological materials (TMs).

References

1. Hasan, M. Z., Kane, C. L. *Reviews of Modern Physics* **82**(4), 3045–3067 https://doi.org/10.1103/RevModPhys.82.3045(2010).
2. Bansil, A., Lin, H., Das, T. *Reviews of Modern Physics* **88**(2) https://doi.org/10.1103/RevModPhys.88.021004 (2016).
3. Gong, P.-L. *et al.* Robust and pristine topological Dirac semimetal phase in pressured two-dimensional black phosphorus. *J. Phys. Chem. C* **121**, 20931–20936 (2017).
4. Chen, C., Su, Z., Zhang, X., Chen, Z. & Sheng, X.-L. From multiple nodal chain to Dirac/Weyl semimetal and topological insulator in ternary hexagonal materials. *J. Phys. Chem. C* **121**, 28587–28593 (2017).
5. Hsu, C.-H., Sreeparvathy, P. C., Barman, C. K., Chuang, F.-C. & Alam, A. Coexistence of topological nontrivial and spin-gapless semiconducting behavior in $MnPO_4$: a composite quantum compound. *Phys. Rev. B* **103**, 195143 (2021).
6. Yang, B.-J. & Nagaosa, N. Classification of stable three-dimensional Dirac semimetals with nontrivial topology. *Nat. Commun.* **5**, 4898 (2014).
7. Wing Chi, Yu Xiaoting, Zhou Feng-Chuan, Chuang Shengyuan A., Yang Hsin, Lin Arun, Bansil.*Physical Review Materials* **2**(5) https://doi.org/10.1103/PhysRevMaterials.2.051201(2018).
8. Armitage, N. P., Mele, E. J. & Vishwanath, A. Weyl and Dirac semimetals in three-dimensional solids. *Rev. Mod. Phys.* **90**, 015001 (2018).
9. Rober, E., Hackstein, K., Coufal, H. & Sotier, S. Magnetic-susceptibility of liquid Na1-Xbix alloys. *Phys. Status Solidi B Basic Res.* **93**, K99-102 (1979).
10. Koshino, M. & Ando, T. Anomalous orbital magnetism in Dirac-electron systems: Role of pseudospin paramagnetism. *Phys. Rev. B* **81**, 195431 (2010).
11. Abrikosov, A. A. Quantum magnetoresistance. *Phys. Rev. B* **58**, 2788–2794 (1998).
12. Zhang, W. *et al.* Topological aspect and quantum magnetoresistance of β-Ag_2Te. *Phys. Rev. Lett.* **106**, 156808 (2011).
13. Xiong, J. *et al.* Evidence for the chiral anomaly in the Dirac semimetal Na_3Bi. *Science* **350**, 413–416 (2015).
14. Li, H. *et al.* Negative magnetoresistance in Dirac semimetal Cd_3As_2. *Nat. Commun.* **7**, 10301 (2016).
15. Liu, C.-X. *et al.* Oscillatory crossover from two-dimensional to three-dimensional topological insulators. *Phys. Rev. B* **81**, 041307 (2010).
16. Wang, Z. *et al.* Dirac semimetal and topological phase transitions in A_3Bi (A = Na, K, Rb). *Phys. Rev. B* **85**, 195320 (2012).
17. Wang, Z., Weng, H., Wu, Q., Dai, X. & Fang, Z. Three-dimensional Dirac semimetal and quantum transport in Cd_3As_2. *Phys. Rev. B* **88**, 125427 (2013).
18. Liu, Z. K. *et al.* A stable three-dimensional topological Dirac semimetal Cd_3As_2. *Nat. Mater.* **13**, 677–681 (2014).
19. Neupane, M. *et al.* Observation of a three-dimensional topological Dirac semimetal phase in high-mobility Cd_3As_2. *Nat. Commun.* **5**, 3786 (2014).
20. He, L. P. *et al.* Quantum transport evidence for the three-dimensional Dirac semimetal phase in Cd_3As_2. *Phys. Rev. Lett.* **113**, 246402 (2014).
21. Liu, Z. K. *et al.* Discovery of a three-dimensional topological Dirac semimetal, Na_3Bi. *Science* **343**, 864–867 (2014).
22. Huang, H., Zhou, S. & Duan, W. Type-II Dirac fermions in the $PtSe_2$ class of transition metal dichalcogenides. *Phys. Rev. B* **94**, 121117 (2016).
23. Zhang, K. *et al.* Experimental evidence for type-II Dirac semimetal in $PtSe_2$. *Phys. Rev. B* **96**, 125102 (2017).
24. Liu, Y. *et al.* Identification of topological surface state in $PdTe_2$ superconductor by angle-resolved photoemission spectroscopy. *Chin. Phys. Lett.* **32**, 067303 (2015).
25. Noh, H.-J. *et al.* Experimental realization of type-II Dirac fermions in a $PdTe_2$ superconductor. *Phys. Rev. Lett.* **119**, 016401 (2017).
26. Yan, M. *et al.* Lorentz-violating type-II Dirac fermions in transition metal dichalcogenide $PtTe_2$. *Nat. Commun.* **8**, 257 (2017).
27. Meng-Kai, Lin Rovi Angelo B., Villaos Joseph A., Hlevyack Peng, Chen Ro-Ya, Liu Chia-Hsiu, Hsu José, Avila Sung-Kwan, Mo Feng-Chuan, Chuang T.-C., Chiang *Physical Review Letters* **124**(3), https://doi.org/10.1103/PhysRevLett.124.036402(2020).
28. Xu, C. *et al.* Topological type-II Dirac fermions approaching the fermi level in a transition metal dichalcogenide $NiTe_2$. *Chem. Mater.* **30**, 4823–4830 (2018).
29. Ghosh, B. *et al.* Observation of bulk states and spin-polarized topological surface states in transition metal dichalcogenide Dirac semimetal candidate $NiTe_2$. *Phys. Rev. B* **100**, 195134 (2019).
30. Mukherjee, S. *et al.* Fermi-crossing Type-II Dirac fermions and topological surface states in $NiTe_2$. *Sci. Rep.* **10**, 12957 (2020).
31. Hlevyack, J. A. *et al.* Dimensional crossover and band topology evolution in ultrathin semimetallic $NiTe_2$ films. *NPJ 2D Mater. Appl.* **5**, 1–9 (2021).
32. Paul Albert L., Sino Liang-Ying, Feng Rovi Angelo B., Villaos Harvey N., Cruzado Zhi-Quan, Huang Chia-Hsiu, Hsu Feng-Chuan, Chuang. Anisotropic Rashba splitting in Pt-based Janus monolayers PtXY (XY = S Se or Te). *Nanoscale Advances* **3**(23), 6608–6616 https://doi.org/10.1039/D1NA00334H (2021).

33. Rovi Angelo B., Villaos Christian P., Crisostomo Zhi-Quan, Huang Shin-Ming, Huang Allan Abraham B., Padama Marvin A., Albao Hsin, Lin Feng-Chuan, Chuang. Thickness dependent electronic properties of Pt dichalcogenides. npj 2D Materials and Applications **3**(1) https://doi.org/10.1038/s41699-018-0085-z(2019).

34. Liang-Ying, Feng Rovi Angelo B., Villaos Zhi-Quan, Huang Chia-Hsiu, Hsu Feng-Chuan, Chuang. Layerdependentband engineering of Pd dichalcogenides: a first-principles study. *New Journal of Physics* **22**(5), 053010. https://doi.org/10.1088/1367-2630/ab7d7a (2020).

35. Jiangming, Cao Zhi-Quan, Huang Gennevieve, Macam Yifan, Gao Naga Venkateswara Rao, Nulakani Xun, Ge Xiang, Ye Feng-Chuan, Chuang Li, Huang Prediction of massless Dirac fermions in a carbon nitride covalent network. *Applied Physics Letters* **118**(13), 133104. https://doi.org/10.1063/5.0046069 (2021).

36. Feng, L-Y., *et al.* Magnetic and topological properties in hydrogenated transition metal dichalcogenide monolayers. *Chinese J. Physics* https://doi.org/10.1016/j.cjph.2020.03.018 (2020).

37. Zhi-Quan, Huang Chia-Hsiu, Hsu Christian P., Crisostomo Gennevieve, Macam Jing-Rong, Su Hsin, Lin Arun, Bansil Feng-Chuan, Chuang. Quantum anomalous Hall insulator phases in Fe-doped GaBi honeycomb. *Chinese Journal of Physics* 67246–252 https://doi.org/10.1016/j.cjph.2020.07.007 (2020).

38. Ali, Sufyan Gennevieve, Macam Chia-Hsiu, Hsu Zhi-Quan, Huang Shin-Ming, Huang Hsin, Lin Feng-Chuan, Chuang. Theoretical prediction of topological insulators in two-dimensional ternary transition metal chalcogenides (MM'X4 M = Ta Nb or V; M'= Ir Rh or Co; X = Se or Te). *Chinese Journal of Physics* 7395–102 https://doi.org/10.1016/j.cjph.2021.06.014 (2021).

39. Gennevieve, Macam Ali, Sufyan Zhi-Quan, Huang Chia-Hsiu, Hsu Shin-Ming, Huang Hsin, Lin Feng-Chuan, Chuang. *Applied Physics Letters* **118**(11), 111901. https://doi.org/10.1063/5.0036838 (2021).

40. Aniceto B., Maghirang Zhi-Quan, Huang Rovi Angelo B., Villaos Chia-Hsiu, Hsu Liang-Ying, Feng Emmanuel, Florido Hsin, Lin Arun, Bansil Feng-Chuan, Chuang. Predicting two-dimensional topological phases in Janus materials by substitutional doping in transition metal dichalcogenide monolayers. npj 2D Materials and Applications **3**(1) https://doi.org/10.1038/s41699-019-0118-2 (2019).

41. Feng-Chuan, Chuang Chia-Hsiu, Hsu Hsin-Lei, Chou Christian P., Crisostomo Zhi-Quan, Huang Shih-Yu, Wu Chien-Cheng, Kuo Wang-Chi V., Yeh Hsin, Lin Arun, Bansil. Prediction of two-dimensional topological insulator by forming a surface alloy on Au/Si(111) substrate. *Physical Review B* **93**(3) https://doi.org/10.1103/PhysRevB.93.035429 (2016).

42. Zi'Ang, Gao Chia-Hsiu, Hsu Jing, Liu Feng-Chuan, Chuang Ran, Zhang Bowen, Xia Hu, Xu Li, Huang Qiao, Jin Pei Nian, Liu Nian, Lin. Synthesis and characterization of a single-layer conjugated metal–organic structure featuring a non-trivial topological gap. *Nanoscale* **11**(3), 878–881 https://doi.org/10.1039/C8NR08477G (2019).

43. Guloy, A.M. Chemistry, structure, and bonding of Zintl phases and ions Edited by Susan M. Kauzlarich (University of California-Davis). VCH Publishers, Inc.: New York, Weinheim and Cambridge. 1996. $125.00. xxx + 306 pp. ISBN 1-56081-900-6. *J. Am. Chem. Soc.* **120,** 7663–7663 (1998).

44. Peng, W., Chanakian, S. & Zevalkink, A. Crystal chemistry and thermoelectric transport of layered AM2X2 compounds. *Inorg. Chem. Front.* **16**, 1744–1759 (2018).

45. Kauzlarich, S.M., Zevalkink, A., Toberer, E., & Snyder, G.J. Chapter 1:Zintl phases: recent developments in thermoelectrics and future outlook. *Thermoelect. Mater. Dev.* pp 1–26 (2016)

46. Xu, N., Xu, Y. & Zhu, J. Topological insulators for thermoelectrics. *NPJ Quant. Mater.* **2**, 1–9 (2017).

47. Gui, X. *et al.* A new magnetic topological quantum material candidate by design. *ACS Cent. Sci.* **5**, 900–910 (2019).

48. Ma, J. *et al.* Emergence of nontrivial low-energy Dirac fermions in antiferromagnetic EuCd$_2$As$_2$. *Adv. Mater.* **32**, 1907565 (2020).

49. Xu, Y., Song, Z., Wang, Z., Weng, H. & Dai, X. Higher-order topology of the Axion insulator EuIn$_2$As$_2$. *Phys. Rev. Lett.* **122**, 256402 (2019).

50. Wang, H. *et al.* A magnetic topological insulator in two-dimensional EuCd$_2$Bi$_2$: giant gap with robust topology against magnetic transitions. *Mater. Horiz.* **8**, 956–961 (2021).

51. Wang, L.-L., Kaminski, A., Canfield, P. C. & Johnson, D. D. Different topological quantum states in ternary Zintl compounds: BaCaX (X = Si, Ge, Sn and Pb). *J. Phys. Chem. C* **122**, 705–713 (2018).

52. Essin, A. M., Moore, J. E. & Vanderbilt, D. Magnetoelectric polarizability and axion electrodynamics in crystalline insulators. *Phys. Rev. Lett.* **102**, 146805 (2009).

53. Varnava, N. & Vanderbilt, D. Surfaces of axion insulators. *Phys. Rev. B* **98**, 245117 (2018).

54. Kranenberg, C. *et al.* New compounds of the ThCr$_2$Si$_2$-type and the electronic structure of CaM$_2$Ge$_2$ (M: Mn–Zn). *J. Solid State Chem.* **167**, 107–112 (2002).

55. He, Y. *et al.* SymTopo: An automatic tool for calculating topological properties of nonmagnetic crystalline materials. *Chin. Phys. B* **28**, 13 (2019).

56. Perez, M. N. R. *et al.* Quantum spin Hall insulating phase and van Hove singularities in Zintl single-quintuple-layer AM2X (A = Ca, Sr, or Ba; M = Zn or Cd; X = Sb or Bi) family. *Appl. Phys. Rev.* **9**, 011410 (2022).

57. Saal, J. E., Kirklin, S., Aykol, M., Meredig, B. & Wolverton, C. Materials design and discovery with high-throughput density functional theory: the open quantum materials database (OQMD). *JOM* **65**, 1501–1509 (2013).

58. Kirklin, S. *et al.* The open quantum materials database (OQMD): assessing the accuracy of DFT formation energies. *NPJ Comput. Mater.* **1**, 1–15 (2015).

59. Mewis, A. AB2X2 compounds with the CaAl$_2$Si$_2$ structure, IV [1] the crystal structure of CaZn$_2$Sb$_2$, CaCd$_2$Sb$_2$, SrZn$_2$Sb$_2$, and SrCd$_2$Sb$_2$. *Z. Für Naturforschung B* **33**, 382–384 (1978).

60. Vergniory, M. G. *et al.* A complete catalogue of high-quality topological materials. *Nature* **566**, 480–485 (2019).

61. Zhang, T. *et al.* Catalogue of topological electronic materials. *Nature* **566**, 475–479 (2019).

62. Jain, A. *et al.* Commentary: the materials project: a materials genome approach to accelerating materials innovation. *APL Mater.* **1**, 011002 (2013).

63. Hsu, C.-H. *et al.* Two-dimensional topological crystalline insulator phase in Sb/Bi planar honeycomb with tunable Dirac gap. *Sci. Rep.* **6**, 18993 (2016).

64. Yu, Z.-M., Zhang, Z., Liu, G.-B., Wu, W., Li, X.-P., Zhang, R.-W., Yang, S.A., & Yao, Y. Encyclopedia of emergent particles in three-dimensional crystals *ArXiv210201517Cond-Mat* (2021)

65. Blöchl, P. E. Projector augmented-wave method. *Phys. Rev. B* **50**, 17953–17979 (1994).

66. Kresse, G. & Joubert, D. From ultrasoft pseudopotentials to the projector augmented-wave method. *Phys. Rev. B* **59**, 1758–1775 (1999).

67. Perdew, J. P., Burke, K. & Ernzerhof, M. Generalized gradient approximation made simple. *Phys. Rev. Lett.* **77**, 3865–3868 (1996).

68. Togo, A. & Tanaka, I. First principles phonon calculations in materials science. *Scr. Mater.* **108**, 1–5 (2015).

69. Krukau, A. V., Vydrov, O. A., Izmaylov, A. F. & Scuseria, G. E. Influence of the exchange screening parameter on the performance of screened hybrid functionals. *J. Chem. Phys.* **125**, 224106 (2006).

70. Pizzi, G. *et al.* Wannier90 as a community code: new features and applications. *J. Phys. Condens. Matter* **32**, 165902 (2020).

71. Wu, Q., Zhang, S., Song, H.-F., Troyer, M. & Soluyanov, A. A. WannierTools: an open-source software package for novel topological materials. *Comput. Phys. Commun.* **224**, 405–416 (2018).

Author contributions

L. Y. F. performed the first-principles calculation. L. Y. F., R. A. B. V., A. B. M. III, Z. Q. H., and C. H. H. interpreted and analyzed the data. F. C. C. initiated and supervised the whole study. All the authors wrote the paper together.

Competing interests

The authors declare no competing interests.

Additional information

Supplementary Information The online version contains supplementary material available at https://doi.org/10.1038/s41598-022-08370-2.

Correspondence and requests for materials should be addressed to F.-C.C.

Reprints and permissions information is available at www.nature.com/reprints.

Publisher's note Springer Nature remains neutral with regard to jurisdictional claims in published maps and institutional affiliations.